SUST J Sci Tech, Vol 30(1) 2020, 32 – 39 ISSN 1682-895X

Numerical Simulation of Blood Flow through Stenosed Artery Using Bifurcation Concept

(Submitted : 30.11.2019 ; Accepted : 25.06.2020)

Md. Alamgir Kabir[1*], Md. Shafiqul Islam[2], Md. Ferdous Alam[2], Md. Ashraf Uddin[1]

[1]Department of Mathematics, Shahjalal University of Science and Technology, Sylhet-3114, Bangladesh
[2]Department of Mechanical Engineering, Shahjalal University of Science and Technology, Sylhet-3114, Bangladesh
[*]Corresponding Author's Email:akabir-mat@sust.edu

Abstract

Blood flow patterns are extensively associated with the initial development of atherosclerosis in the bifurcation of the carotid artery. In the present study, two different arterial bifurcation geometrical models are used to investigate the hemodynamic parameters numerically. Model 1 is assumed as a bifurcated carotid artery without stenosis whereas Model 2 with stenosis. The inlet boundary conditions for the streamwise velocity have been created by the equation of sinusoidal pulsatile velocity profile and the program is written in C-language using the interface of User Defined Function (UDF) of Fluent and linked with the solver. Blood is considered as non –Newtonian fluid and in this computation widely known Carreau model has been used to describe the non- Newtonian behavior of blood. To capture, the turbulent features of the flow, k-ω turbulence model has been used. Our study found that due to the presence of stenosis, a huge pressure drop (~13332 Pa) occurs at the throat of the stenosis that can cause the potential damage of the artery. The maximum velocity (~0.29 m/s) and wall shear (~5.11 Pa) has also been found at the throat of the stenosis which is much higher than (~31.82% and 61.20%, respectively) that of the artery without stenosis.

Keywords: stenosis; artery; Navier-Stokes; simulation; heart disease

1. Introduction

The cardiovascular system plays an important role in transporting nutrients and waste throughout the body. Cardiovascular diseases cause the majority of deaths reported in developed countries. Earlier, most of the cardiovascular diseases affected the aged group of people, but that situation is different now. There are several other risk factors for heart diseases like age, gender, use of tobacco, high blood pressure and cholesterol, etc. causing the development of stenosis [1]. Atherosclerosis is a disease narrowing a coronary artery due to plaque buildup. Generally, there is no symptom until it severely narrows the artery causing serious problems including heart attack, stroke, or even death [2].

A detrimental fibro-fatty plaque formation in human arteries reduces the normal path of the blood flow. This obstruction in the artery creates disturbances of the normal flow in arterial branches and at curvatures which initiate the development and progression of atherosclerosis. Although the mechanism of atherosclerotic plaque development is not well known, atherosclerotic plaques occur in particular vasculatures such as carotid artery and coronary artery including branching vessel, bifurcation, and curves [3]. According to the statistical survey, it was found that stenosis is usually seen at the arterial bifurcations particularly in the common coronary artery (CCA), bifurcation of the carotid artery, branches on the aortic arch and abdominal aorta. As the locations of preliminary progress of atherosclerosis are commonly connected with regions toward flow recirculation and separation at the bifurcation and the inner curvature's wall, the blood flow patterns in bifurcations and curvatures are of interest in the study of atherogenesis. Even though significant improvements have been made in vitro by using flow visualization techniques or lager Doppler anemometry, blood flow behaviors in arteries, particularly in bifurcation areas and curvatures regions is still now beyond the understanding in details. To investigate the region of the recirculation and separated flow in curvatures and bifurcations, a large number of studies have been carried out to analyze the blood flow.

For example, Seo [3] conducted numerical simulations of blood flow in arterial bifurcation models. In the study, two different arterial bifurcation model geometries were

used in the flow simulation. Otero-Cacho, Aymerich [4] determined the hemodynamic risk for vascular disease in planar artery bifurcations. More specifically this study helps in understanding hemodynamics in blood circulation which is crucial to unveil the mechanisms underlying the formation of stenosis and atherosclerosis. Chen and Lu [5] performed a numerical investigation of the non-Newtonian pulsatile blood flow in a bifurcation model with a non-planar branch. However, with the advent of recent supercomputers and rapid advancement of computational fluid dynamics (CFD) techniques, computer modeling to analyze the blood flow has been playing an increasing role.

This study aims to perform numerical simulations to get blood flow characteristics through arteries using the bifurcation concept. Blood flow patterns are extensively associated with the initial development of atherosclerosis in the bifurcation of the carotid artery. Although few works have been carried out including the influence of non-Newtonian properties, among them Chen et al. [6] conducted their study on the non-Newtonian properties of blood in the rigid model of the carotid bifurcation under pulsatile flow condition. Gupta [7] and Sharzehee, Khalafvand [8] investigated the flow field in the carotid artery assuming the fluid-structure interaction and the comparison between Newtonian and non-Newtonian fluid. Kabir et al. [9] numerically studied the effects of Reynolds number on blood flow with spiral velocity through regular arterial stenosis. A further study on the simulation of a regular artery and arteries with single and multiple stenoses has been carried out by Kabir et al. later [10]. However, a complete understanding of the bifurcated artery along with stenosis is still missing. Thus, two different arterial bifurcation geometrical models are used to investigate the hemodynamic parameters numerically. Model 1 is assumed as a bifurcated carotid artery without stenosis whereas Model 2 is considered with stenosis.

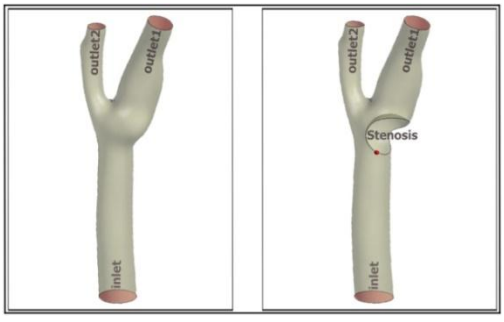

Figure 1: Model bifurcated geometry (with stenosis (right) without stenosis (left)).

The objective of this study is to examine the blood flow phenomena through arterial bifurcation to gain a proper understanding of the flow characteristics that initiates the development of atherosclerosis through the artery. Through a better understanding of the flow mechanisms about how atherosclerosis will instigate, grow up, and rapture, clinicians will be capable to predict how to treat such type of diseases.

2. Model geometry

Bifurcation model arteries are considered for these simulations. This artery has one inlet and two outlets shown in Figure 1. The two outlets have different diameters. The larger outlet has a diameter of about 4.45mm while the diameter of the smaller outlet is about 3.05mm. The inlet diameter of the artery is about 6.25mm. Initially, a bifurcation artery without stenosis is considered whose volume is 1875.8 mm^3 and the surface area of this artery is 1324.5 mm^2. The surface area of the inlet is 30.98 mm^2 and the larger outlet is 14.83 mm^2 while the smaller outlet has a surface area of 7.23 mm^2. In the later part of this simulation, stenosis is considered in the region where the artery gets bifurcated into two outlets of different diameters. The stenosis causes a reduction in the volume of the artery. The radius of this spherical region is taken as 3.00mm. The surface area of this region is 76.13 mm^2. However, due to the presence of stenosis, there occurs a significant reduction in the total volume of the artery. The total volume is 1749.5 mm^3 and the surface area is 1341.4 mm^2. Thus, the total volume reduces about 6.75% of the original volume.

3. Flow governing equations

In this study, the Reynolds averaged Navier-Stokes (RANS) equations, the turbulent eddy viscosity, the standard model, and their relevant equations are used as governing equations for the simulations. After applying the Reynolds time-averaging techniques, the Reynolds averaged Navier–Stokes (RANS) are obtained as tensor form, given as follows [11]:

$$\frac{\partial \mathrm{u}_\mathrm{i}}{\partial \mathrm{x}_\mathrm{i}} = 0 \qquad (1)$$

$$\frac{\partial}{\partial t}\left(\rho u_i\right) + \frac{\partial}{\partial x_j}\left(\rho u_i u_j\right) = -\frac{\partial p}{\partial x_i} + \frac{\partial}{\partial x_j}\left[\mu\left(\frac{\partial u_i}{\partial x_j} + \frac{\partial u_j}{\partial x_i}\right)\right] + \frac{\partial \tau_{ij}}{\partial x_j} \qquad (2)$$

Where, $x_i = (x, y, z)$ are the Cartesian co-ordinate systems, u_i are the mean velocity components, ρ is the density, p is the pressure and τ_{ij} is the Reynolds stress (wall shear stress).

SUST J Sci Tech, Vol 30(1) 2020, 32 – 39

The Boussinesq hypothesis is employed to model the Reynolds stress τ_{ij} which is given as follows:

$$\tau_{ij} = -\rho\langle u'_i u'_j \rangle = \mu_t \left(\frac{\partial u_i}{\partial x_j} + \frac{\partial u_j}{\partial x_i} \right) - \frac{2}{3}\rho k \delta_{ij} \quad (3)$$

where, u'_i is the fluctuating velocity components, $k = \frac{1}{2}\langle u'_i u'_j \rangle$ is the turbulent kinetic energy and μ_t is the turbulent eddy viscosity obtained by employing the standard $k-\omega$ model of Wilcox [12]. The main objective of the Boussinesq hypothesis is to relate the Reynolds stresses to the mean velocity gradients. In the $k-\omega$ model, the eddy-viscosity is modeled as:

$$\mu_t = \frac{\rho k}{\omega} \quad (4)$$

Where, ω is the specific dissipation rate which can also be considered as the ratio of dissipation rate (ε) to turbulence kinetic energy (k).

Here k and ω are obtained from the following equations:

$$\frac{\partial k}{\partial t} + \frac{\partial k\langle u_j \rangle}{\partial x_j} = -\frac{1}{\rho}\langle \rho u'_i u'_j \rangle \frac{\partial \langle u_i \rangle}{\partial x_j} - \beta^* k\omega + \frac{\partial}{\partial x_j}\left[\frac{1}{\rho}\left(\mu + \sigma^* \mu_t\right) \frac{\partial k}{\partial x_j} \right] \quad (5)$$

$$\frac{\partial \omega}{\partial t} + \frac{\partial \omega\langle u_j \rangle}{\partial x_j} = -\alpha_1 \frac{\omega}{\rho k}\langle \rho u'_i u'_j \rangle \frac{\partial \langle u_i \rangle}{\partial x_j} - \beta\omega^2 + \frac{\partial}{\partial x_j}\left[\frac{1}{\rho}\left(\mu + \sigma\mu_t\right) \frac{\partial \omega}{\partial x_j} \right] \quad (6)$$

Where, σ* = 0.5, ß* = 0.072, σ = 0.5, α_1 = 1.0, ß = 0.072

It can be mentioned that $k-\omega$ model provides a better result for blood flow. While other models are unable to capture small drops and peaks of blood flow, this model can capture large scale variation in different parameters of blood flow.

4. Non-Newtonian model

Blood of the human body contains two parts i.e. liquid and solid parts. The liquid part of the blood is called plasma which generally consists of water, salts, and protein. Since over 50% of blood in the human body is plasma, blood is considered as incompressible and Newtonian-homogeneous fluid with a density (ρ) of 1060 kg/m^3 and a constant dynamic viscosity (μ) of 3.71×10^{-3} Pa s. But in the microcirculatory system such as small branches and capillaries, blood exhibits non - Newtonian behavior. Considering such nature of blood, several models have been developed which can capture the non-Newtonian behavior of blood. In the present study, the well-known Carreau model [13] has been used to capture the non-Newtonian behavior of the fluid and the model is defined as:

$$\mu\left(\left|\dot{\gamma}\right|\right) = \mu_\infty + \left(\mu_0 - \mu_\infty\right)\left[1 + \left(\lambda\dot{\gamma}\right)^2\right]^{(n-1)/2} \quad (7)$$

Where, μ_∞ =0.00345Pa s is the infinite shear viscosity, μ_0=0.056 Pa s is the blood viscosity at zero shear rate, γ is the instantaneous shear rate, λ=3.313 s is the time constant which is associated with the viscosity that changes with shear rate and n=0.3568 is the power-law index.

5. Boundary condition

At the inlet of the models, a sinusoidal pulsatile velocity profile has been used. The pulsatile profile within each period is considered to be a combination of two phases. The velocity at the inlet varies in a sinusoidal pattern during the systolic phase. The considered outlet pressure is 13332 Pa and no-slip boundary condition is considered in the wall.

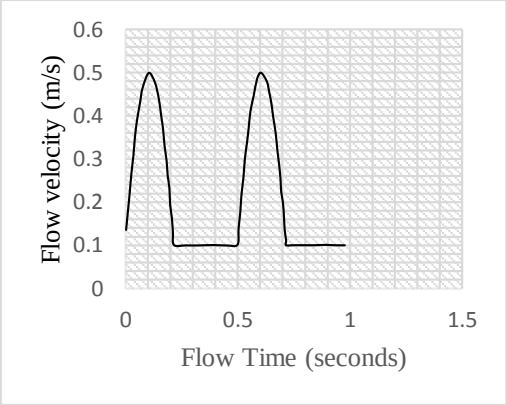

Figure 2: Pulsatile inlet velocity profile (two Periods)

$$V_{inlet}(t) = \begin{cases} 0.5\sin[4\pi(1+0.0160236)] : 0.5n < t \le 0.5n + 0.218 \\ 0.1 : 0.5n + 0.218 < t \le 0.5(n+1) \end{cases}$$

$$n = 0, 1, 2, ...$$

6. Computational procedure

Fluent [14] has been used to perform the simulations of the current study which incorporates finite volume method intending to discretize the governing equations (1, 2) and forms a system of algebraic equations that is solved by an iterative process. For the coupling of velocity with pressure, the SIMPLE method of Patankar [15] is used. For the process of discretization, the second-order upwind scheme is employed for the equations of momentum, turbulent kinetic energy (k), and specific dissipation rate (ω). On the contrary, the second-order accurate scheme is employed for the Poisson-like pressure equation.

Pressure based solver is used to solve the discretized algebraic equations. The default values are used for the

under relaxation factors for pressure, momentum, and *k-ω* equations. The inlet boundary conditions for the stream wise velocity are written in C-language using the interface of User Defined Function (UDF) of Fluent and linked with the solver. Arbitrary values of the velocity components and *k-ω* are used to initiate the solution process. The minimum time step size used for the simulation was $1x10^{-4}$sec with 10000 numbers of total steps. The maximum iterations were 20 per each time step to collect the statistical data. The residuals are monitored regularly. A strong indicator for stable and accurate solutions is the decrement of the magnitude of the residuals and residuals dropped gradually. The iteration process is called off when the residuals reach 10^{-6}. Actually, beyond this level, the residuals don't depend on the iteration number and the converged solutions are obtained.

7. Grid independency test

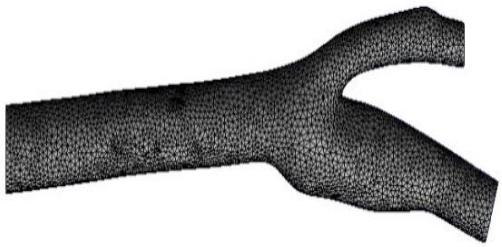

Figure 3(a): Grid distribution for model artery.

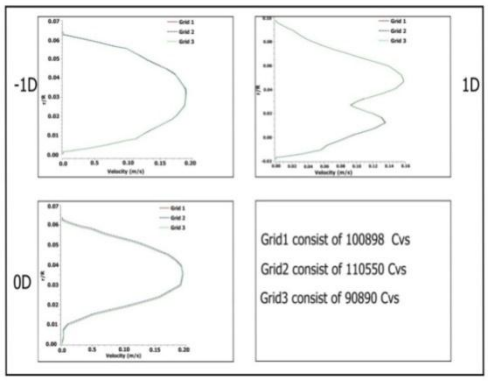

Figure 3(b): Grid independency test for three different grids for velocity profiles

The total computational domain is discretized in three different grids i.e. Grid 1, Grid 2, and Grid 3 respectively. Grid 1 consists of 100898 control volume sand Grid 2 consists of 110550 control volumes while Grid 3 consists of 90890 control volumes. To check the sensitivity of the numerical results, the velocity profiles at three different axial positions are considered for Grid 1, Grid 2, and Grid 3. The findings from three different grids revealed that the velocity profiles do not differ significantly for the existing simulations. This suggests that the numerical simulation results do not depend on grid arrangements that have been chosen for the present study.

8. Results and discussion

The variation in pressure in two geometrical models is shown in figure 4. Model 1 indicates the artery without stenosis and Model 2 indicates the artery with stenosis. In general, the magnitudes of pressure are high at the upstream region of the artery and the pressure patterns severely change due to both the branching and curvature effects near the divider wall. In the artery without stenosis after the branching, the pressure becomes low.

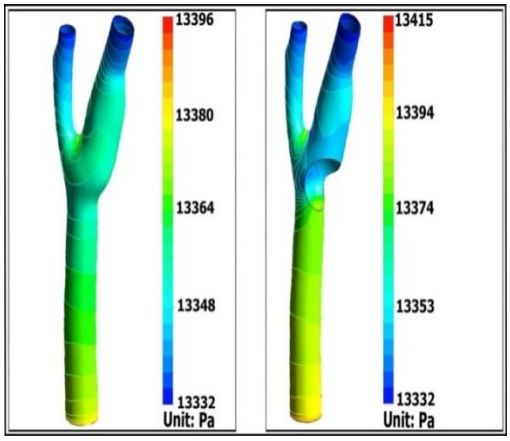

Figure 4: Variation in the pressure along the artery with stenosis (right) and without stenosis (left).

Similarly, in the artery with stenosis after the branching, the pressure also becomes low. That is, in the presence of branching of the artery, a great amount of pressure drop occurs in the bifurcated region. However, if we compare the variation in pressure along the artery with stenosis and without stenosis, it is clear that the drop of pressure is larger after the branching in the artery with stenosis compared to the artery without stenosis. It is important to note that the larger drop in pressure occurs after the stenosis region which can significantly affect the epithelial cells of the artery. The upstream pressure for the artery without stenosis is around 13380 Pa which reduces to around 13364 Pa at the bifurcated region. On the other hand, the upstream pressure of the artery with stenosis is around 13400 Pa. Due to stenosis, it reduces to around 13332 Pa at the throat of the stenosis. The numerical values suggest almost 4 times pressure drop for the presence of the stenosis. A comparative study has been done by Manjunath, Shetty [16] where they compared the analytical results from the model with that

of the experimental values for pressure with the bifurcation model arteries. Moreover, the results obtained from our study are also similar to the results of Debbich and Abdallah [17] and Tan, Soloperto [18]. Ladak, Thomas [19] studied the pressure behavior in a stenosed artery and results are in line with this study. As the initial outlet pressure was considered 13332 Pa, therefore the variation of pressure for both of the cases is significant. The maximum pressure is found in the upstream zone as well as in the bifurcated region and slightly large in the case of the artery with stenosis. The minimum pressure remains the same in both the artery models and the minimum pressure is observed at the outlet for both cases.

Streamline velocity is shown in figure 5. Model 2 indicates the artery with stenosis and Model 1 indicates the artery without stenosis. The flow divides symmetrically into both vessels, and this can also be observed in the stream velocity profiles. In general, the magnitudes of streamline velocity are high through the artery and the velocity severely changes due to both the branching and curvature effects near the divider wall. In the artery without stenosis, after the branching in the downstream region, the streamline velocity becomes higher and a light twisting effect has been observed. Similarly, in the artery with the stenosis after the branching in the downstream region, the velocity also becomes higher. However, this high velocity is not as higher as in the artery without stenosis. In the artery with a stenosis, the velocity at the bifurcation region is higher and at the throat of stenosis, the intensity of velocity is much higher. The streamline velocity right after the bifurcation region is 0.11 m/s for the artery without stenosis while the value is 0.24 m/s for the artery with stenosis. For the artery with the stenosis, the streamline velocity reaches up to 0.25 m/s at the throat of the stenosis.

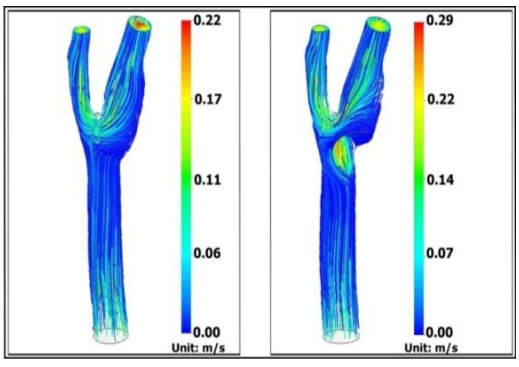

Figure 5: Variation in the streamline velocity along the artery with stenosis (right) and without stenosis (left).

Interestingly, the twisting effect is much more in the artery without stenosis. However, if the variation is compared in streamline velocity along the artery with stenosis and without stenosis, it is clear that the drop of velocity is larger after the branching in the artery with stenosis compared to the artery without stenosis and strong blood flow circulation has been observed just after the throat of the stenosis and at the bifurcated zone. Thomas Jonathan, Antiga [20], and Sitzer, Puac [21] also found similar behavior of streamline velocity in bifurcated arteries.

Variation in the velocity vector along the artery with stenosis and without stenosis is shown in figure 6(a).

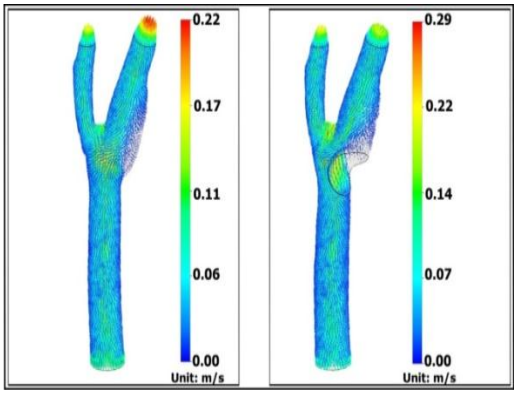

Figure 6(a): Variation in the velocity vector along the artery with stenosis (right) and without stenosis (left).

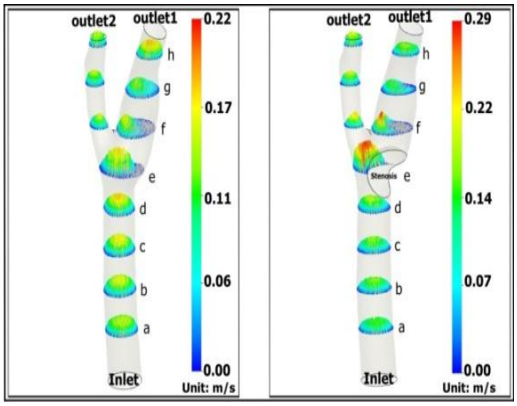

Figure 6(b): Variation in the velocity vector at different positions along the artery with stenosis (right) and without stenosis (left).

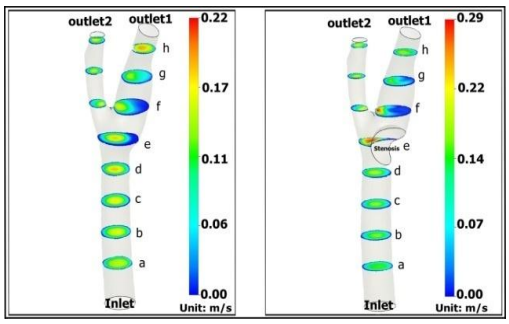

Figure 6(c): Variation in the velocity at different positions along the artery with stenosis (right) and without stenosis (left).

Velocity vector at different locations is shown in figure 6(b) and variation in velocity at different planes towards the direction of flow is shown in figure 6(c).

The minimum velocity was found near the wall arteries for both cases as no-slip boundary condition was considered at the arterial wall. Interestingly, the value of minimum velocity is almost zero just after the throat of the stenosis shown in figure 6(c) at the positions of 6(e), 6(f), and 6(g) for both cases. In the case of the artery without stenosis, the maximum streamwise velocity occurs at the outlet. But for the stenosed artery, the maximum velocity is found at the stenosed area. The maximum streamline velocity significantly increases for the stenosed artery which eventually may cause difficulties. The intensity of the velocity is found maximum at the throat of the stenosis as well as the bifurcated region. Studies of Steinman et al. [22], and Antiga and Steinman [23] are also in line with our findings. Besides, findings of Goubergrits et al. [24] also support this study.

Variation in WSS along the artery with stenosis and without stenosis is illustrated in figure 7. Model 2 indicates the artery with stenosis and Model 1 indicates the artery without stenosis as mentioned earlier. A strong gradient in WSS is observed in the artery with stenosis.

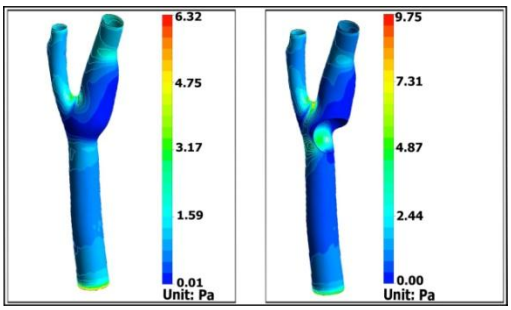

Figure 7: Variation in WSS along the artery with stenosis (right) and without stenosis (left).

However, in the artery without stenosis, the gradient of WSS is not as strong as the artery with stenosis. The WSS is higher before the branching in the artery with stenosis compared to Model 1 with no stenosis as well as strong wall shear stress has been observed at the bifurcated zone for both of the models. For the bifurcation zone, the WSS for Model 1 is around 1.5 Pa while the value is around 4.5 Pa for Model 2.

Because of this high WSS, the internal arterial materials could be damaged. In contrast, the WSS is found comparatively low in the artery with stenosis after the throat of the stenosis which promotes further plaque formation at the branching, and afterward branching, the WSS distributed asymmetrically in both branches in both arteries. The results of this study agree well with Thomas, Milner [25].

The wall shear stress (WSS) significantly changes in the stenosed artery model from the normal model where stenosis is not present. Here, the maximum wall shear stress increases about more than 50% in the case of the stenosed artery which subsequently may create many pathological diseases. The maximum wall shear stress in the stenosed artery occurs at a region just after the stenosis zone near the bifurcation area as well. A comparison of the values of the fluid properties in the artery with stenosis and without stenosis has been shown in table 1.

Table 1: Comparison of different fluid parameters within the artery without stenosis and with stenosis

Fluid Properties (Maximum value)	Without stenosis	With stenosis	%Increase in maximum value of properties
Pressure	13380 Pa	13400 Pa	0.15%
Velocity	0.22 m/s	0.29 m/s	31.82%
Wall shear stress (WSS)	3.17 Pa	5.11 Pa	61.20 %

Table 2: Comparison of different fluid parameters at the position of stenosis for both models From Table 2, it is

Fluid Properties (at throat)	Model 1	Model 2	% of Increase
Pressure drop	15 Pa	68 Pa	353.33%
Velocity	0.11 m/s	0.25 m/s	127.27%
Wall shear stress (WSS)	2.1 Pa	5.11 Pa	143.33 %

easily observed that the fluid properties drastically change for the artery with a stenosis. Pressure drops from 13380 Pa to 13365 Pa for Model 1. On the other hand, pressure drops from 13400 Pa to 13332 Pa for Model 2. Other properties also increase for the presence of a stenosis as shown in table 2 suggesting that the presence of a stenosis may lead to detrimental effects on the human body.

9. Conclusion

The numerical analysis of blood flow through the bifurcated arteries is performed considering both stenosis and without stenosis. The findings of the present study demonstrate that the branching of the artery causes the pressure to increase in the upstream region as well as in the bifurcation zone. This intensity of the pressure is found higher in the stenosed artery compared to the normal artery. The velocity intensity is found maximum at the throat of the stenosed artery. But a huge velocity drop has been found at the bifurcation area near to the wall and the intensity of the velocity drop is very high in the stenosed artery. This sudden velocity drop initiates the flow circulation and flow separation at the post-stenotic region which may propagate further plaque formation. Wall shear stress is also found maximum at the bifurcation region for both of the cases but the intensity of wall stress is much higher in the stenosed artery. This high wall shear can be the cause of the rupturing of the epithelial cells. Moreover, low wall shear stress has been observed at the downstream zone which also can promote additional plaque formation. Thus, by getting a proper insight of the flow mechanisms through the blood vessel, the physicians might be enabled to understand how the atherosclerosis is initiated, grows up and raptures the epithelial cells and thus expose the fatty core inside the vessels and there by they can be able to find out how to treat such type of diseases eventually. Numerical blood flow simulations considering bifurcation concept is well studied. However, studies incorporating bifurcation and stenosis are lacking. The novelty of this paper is inherited in considering arterial stenosis in bifurcated artery. We showed how blood flow behavior changes if we consider stenosis in a bifurcated artery.

References

1. Thomas, B., Sumam, K.S., Blood Flow in Human Arterial System-A Review, Procedia Technology. 2016, 24; 339-346.
2. Kaewbumrung, M., Orankitjaroen, S., Boonkrong, P. et al., Numerical Simulation of Dispersed Particle-Blood Flow in the Stenosed Coronary Arteries, International Journal of Differential Equations. 2018, 2018; 1-16.
3. Seo, T., Numerical simulations of blood flow in arterial bifurcation models, Korea-Australia Rheology Journal. 2013, 25(3); 153-161.
4. Otero-Cacho, Aymerich, A., Flores-Arias, M. T. et al., Determination of hemodynamic risk for vascular disease in planar artery bifurcations, Scientific Reports. 2018, **8**(1); 2795.
5. Chen, J., Lu, X. Y., Numerical investigation of the non-Newtonian pulsatile blood flow in a bifurcation model with a non-planar branch, Journal of Biomechanics. 2006, 39(5); 818-832.
6. Chen, J., Lu, X. Y., Wang, W., Non-Newtonian effects of blood flow on hemodynamics in distal vascular graft anastomoses, Journal of Biomechanics. 2006,39 (11); 1983-1995.
7. Gupta, A.K., Performance and Analysis of Blood Flow through Carotid Artery, International Journal of Engineering Business Management. 2011, 3; 24.
8. Sharzehee, M., Khalafvand, S. S., Han,H.-C.,Fluid-structure interaction modeling of aneurysmal arteries under steady-state and pulsatile blood flow: a stability analysis, Computer methods in biomechanics and biomedical engineering. 2018, 21(3); 219-231.
9. Kabir, M. A., Alam, M.F., Uddin, M. A., A Numerical Study on the Effects of Reynolds Number on Blood Flow with Spiral Velocity Through Regular Arterial Stenosis, Chiang Mai Journal of Science. 2018, 45(6); 2515-2527.
10. Kabir, M. A., Alam, M. F., Uddin, M. A., Numerical Simulation of pulsatile blood flow: A study with normal artery, and arteries with single and multiple stenosis, Egyptsian Jounal of Applied Science Research. 2019.

11. Gabriel, J., Swanson, D. J. A., 1985. ANSYS engineering analysis system user's manual.Swanson Analysis Systems, Houston.
12. Wilcox, D.C., Turbulence Modeling for CFD. DCW Industries, La Cañada, CA. 2004.
13. Carreau, P., Rheological Equations from Molecular Network Theories, Transactions of the Society of Rheology. 1972, 16(1); 99-127.
14. FLUENT 15.0. Tutorials Guide (Free version).
15. Patankar, S.V., Spalding. D.B., A calculation procedure for heat, mass and momentum transfer in three-dimensional parabolic flows, International Journal of Heat and Mass Transfer. 1972, 15(10); 1787–1806.
16. Manjunath, S., Shetty, M., Moon, S., N. J. et al., Arteriovenous Malformation of the Oral Cavity, Case Reports in Dentistry. 2014; 1-5.
17. Debbich, A., Abdallah, A. B., Blood Flow Modeling in a Healthy Carotid Artery Bifurcation: Simulations Against in Vivo Measurements, 2017 IEEE/ACS 14th International Conference on Computer Systems and Applications (AICCSA). 2017.
18. Tan, F.P., Soloperto, G., Bashford, S. et al., Analysis of Flow Disturbance in a Stenosed Carotid Artery Bifurcation Using Two-Equation Transitional and Turbulence Models,Journal of Biomechanical Engineering. 2008, 130(6); 061008-12.
19. Ladak, H.M., Thomas, J. B., Mitchell, J. R. et al., A semi-automatic technique for measurement of arterial wall from black blood MRI, Medical Physics. 2001, 28(6); 1098-1107.
20. Thomas J. B., Antiga, L., Che, S. L. et al., Variation in the Carotid Bifurcation Geometry of Young Versus Older Adults,Stroke. 2005, 36(11); 2450-2456.
21. Sitzer, M., Puac, D., Buehler, A. et al., Internal Carotid Artery Angle of Origin, Stroke. 2003,34(4); 950-955.
22. Steinman, D.A., Thomas, J. B., Ladak, H. M. et al., Reconstruction of carotid bifurcation hemodynamics and wall thickness using computational fluid dynamics and MRI, Magnetic Resonance in Medicine. 2001, 47(1); 149-159.
23. Antiga, L., Steinman, D. A., Robust and objective decomposition and mapping of bifurcating vessels,IEEE Transactions on Medical Imaging. 2004, 23(6); 704-713.
24. Goubergrits, L., Affeld, K.,Fernandez-Britto, J. et al., Atherosclerosis in theHuman Common Carotid Artery. A Morphometric Study of 31 Specimens, Pathology - Research and Practice. 2001, 197(12); 803-809.
25. Thomas, J.B., Milner, J. S., Rutt, B. K. et al., Reproducibility of Image-Based Computational Fluid Dynamics Models of the Human Carotid Bifurcation, Annals of Biomedical Engineering. 2003, 31(2); 132-141.